Anomalous Adsorption of PFAS at the Thin-Water-Film Air-Water Interface in Water-Unsaturated Porous Media

Wenqian Zhang[1] and Bo Guo[1]

[1]Department of Hydrology and Atmospheric Sciences, University of Arizona, Tucson, AZ, USA

Abstract Per- and poly-fluoroalkyl substances (PFAS) are interfacially-active contaminants that adsorb at air-water interfaces (AWIs). Water-unsaturated soils have abundant AWIs, which generally consist of two types: one is associated with the pendular rings of water between soil grains (i.e., bulk AWI) and the other arises from the thin water films covering the soil grains. To date, the two types of AWIs have been treated the same when modeling PFAS retention in vadose zones. However, the presence of electrical double layers of soil grain surfaces and the subsequently modified chemical potential of PFAS at the AWI may significantly change the PFAS adsorption at the thin-water-film AWI relative to that at the bulk AWI. Given that thin water films contribute to over 90% of AWIs in the vadose zone under many field-relevant wetting conditions, it is critical to quantify the potential anomalous adsorption of PFAS at the thin-water-film AWI. We develop a thermodynamic-based mathematical model to quantify this anomalous adsorption. The model couples the chemical equilibrium of PFAS with the Poisson-Boltzmann equation that governs the distribution of electrical potential in a thin water film. Our model analyses suggest that PFAS adsorption at thin-water-film AWI can deviate significantly (up to 82%) from that at bulk AWIs. The deviation increases for lower porewater ionic strength, thinner water film, and higher soil grain surface charge. These results highlight the importance of accounting for the anomalous adsorption of PFAS at the thin-water-film AWI when modeling PFAS fate and transport in the vadose zone.

1. Introduction

Per- and poly-fluoroalkyl substances (PFAS) are emerging contaminants of critical concern. Since the 1940s, PFAS have been used in a variety of applications, which led to their wide presence in the environment (Brusseau et al., 2020; Glüge et al., 2020; Nakayama et al., 2019). Field investigations have demonstrated that PFAS have accumulated significantly in the vadose zone of contamination sites (e.g., D. T. Adamson et al., 2020; Anderson et al., 2019; Brusseau et al., 2020; Dauchy et al., 2019). Most PFAS are surfactants that adsorb at the air-water interface (AWI) (Figure 1a) (e.g., Braun et al., 2017; Kissa, 2001). In the vadose zone, soils contain abundant AWIs due to the coexistence of air and water in the pore spaces. Recent modeling studies (e.g., Gnesda et al., 2022; Guo et al., 2020, 2022; Silva et al., 2020; Wallis et al., 2022; Zeng & Guo, 2021; Zeng et al., 2021) and soil porewater sampling and analysis (Anderson et al., 2022; Brusseau & Guo, 2022; Quinnan et al., 2021; Schaefer et al., 2022) suggest that air-water interfacial adsorption is a major factor contributing to PFAS retention in the vadose zone. It is critical to understand and quantify how adsorption at the AWIs influences PFAS retention in the vadose zone and mass discharge to groundwater.

AWIs in soils can be categorized into two types: one is associated with the pendular rings of water between soil grains and the other arises from the thin water films covering the soil grains (Costanza-Robinson & Brusseau, 2002; Tuller et al., 1999). We refer to the former as bulk AWI and the latter as thin-water-film AWI. To date, adsorption of PFAS at the two types of AWIs has been treated the same in previous studies of PFAS fate and transport in water-unsaturated porous media (e.g., Brusseau et al., 2021; Gnesda et al., 2022; Guo et al., 2020, 2022; Wallis et al., 2022; Zeng & Guo, 2021; Zeng et al., 2021), where PFAS adsorption at AWIs is modeled using a well-established approach from the surfactant literature that combines the Gibbs adsorption equation with the Szyszkowski equation (A. W. Adamson & Gast, 1997; Chang & Franses, 1995; Rosen & Kunjappu, 2012), which is often referred to as the Langmuir-Szyszkowski model.

Many PFAS are ionic and their adsorption at the AWI introduces the so-called electrical double layer (EDL), which comprises two layers of ions with opposite charges—adsorbed PFAS and counterions. The EDL creates an electrical potential gradient across the layers, which may influence PFAS adsorption at the AWI. While the EDL is present at the AWI, the standard Langmuir-Szyszkowski model appears to represent reasonably well the
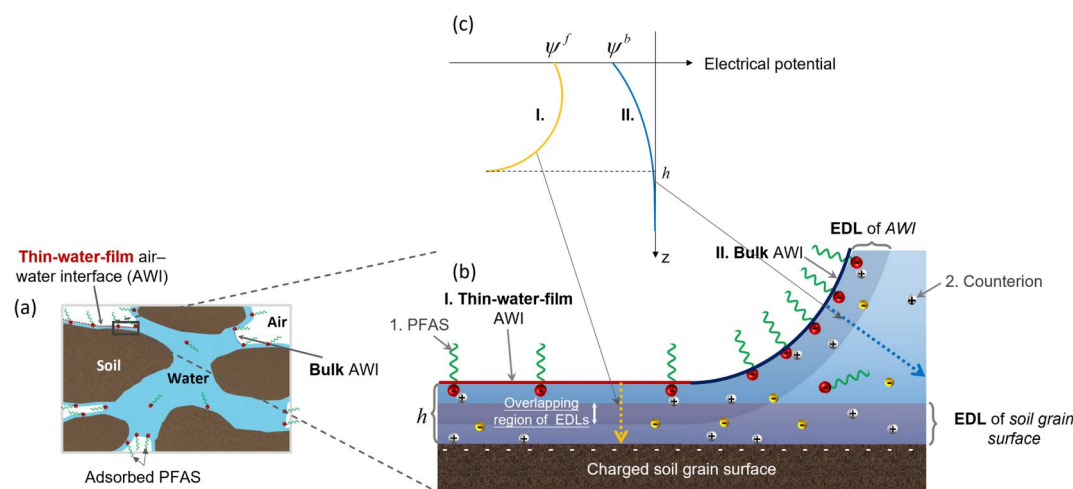
Figure 1. (a) A pore-scale view of per- and poly-fluoroalkyl substances (PFAS) distribution and retention in water-unsaturated soil media: PFAS dissolve in the aqueous phase, adsorb at the solid grain surface, and the bulk and thin-water-film air-water interfaces (AWIs). (b) A zoom-in view of (I) a thin water film AWI connected to (II) a bulk AWI and the distribution of PFAS and ions. The electrical double layers of the AWI and the solid grain surface overlap in the thin water film. An anionic PFAS is used as an example and the solid grain surface is assumed negatively charged. (c) The electrical potential distribution near the thin-water-film AWI compared with that near the bulk AWI. The z-axis represents the distance from the AWI and the h is the thickness of the thin water film. The graphs are not to scale.

adsorption of PFAS and other surfactants at the bulk AWI for the range of conditions reported in the literature to date. For example, the air-water interfacial adsorption coefficients computed by the Langmuir-Szyszkowski model are consistent with direct observation and molecular dynamics simulations of surface adsorption at the bulk AWI (e.g., An et al., 1996; Aveyard, 2019; Brusseau, 2021; Lemay et al., 2023). However, it remains unknown whether the Langmuir-Szyszkowski model is applicable to the AWI of thin water films covering the often charged soil grain surfaces where another EDL arises. Because the thickness of the thin water films can be tens of nanometers or lower (Hamaker, 1937; Israelachvili, 2011; Iwamatsu & Horii, 1996), the EDLs of the soil grain surface and the AWI may overlap (Nishiyama & Yokoyama, 2021; Tokunaga, 2011, 2012). The interaction between the overlapped EDLs is expected to modify the electrical potential at the AWI and the adsorption capacity of PFAS. Consequently, PFAS adsorption at the thin-water-film AWI can deviate significantly from that at bulk AWI. For example, if the solid surface and adsorbed PFAS have the same charge sign (e.g., anionic PFAS and negatively charged soil grain surface), adsorption at the thin-water-film AWI could be smaller than that at a bulk AWI. Conversely, if the solid surface and adsorbed PFAS have opposite charge signs (e.g., cationic PFAS with negatively charged soil grain surface), the adsorption at the thin-water-film AWI could be greater than that at a bulk AWI. In addition to the thin water film thickness, the electrical potential at the AWI is also a function of several other factors, including the amount of interfacial adsorption, ionic strength of the solution, and the charge density of the soil grain surface. To date, the potentially anomalous adsorption of PFAS at the thin-water-film AWI and the primary controlling factors have not been reported in the literature.

Prior studies showed that more than 90% of the AWIs in the vadose zone can arise from the thin water films under most field-relevant wetting conditions (Brusseau et al., 2006, 2007; Costanza-Robinson & Brusseau, 2002; Jiang et al., 2020; Or & Tuller, 1999). Consequently, it is anticipated that the AWIs associated with thin water films are a major contributor to PFAS retention in the vadose zone. Therefore, understanding the primary factors controlling the anomalous adsorption of PFAS at the thin-water-film AWI is critical. Furthermore, it is also important to identify conditions under which the anomalous adsorption at thin-water-film AWI is significant or irrelevant for predicting PFAS retention in the vadose zone and mass discharge to groundwater at field contamination sites.

The present study develops a theoretical framework to comprehensively understand and quantify the potentially anomalous adsorption of PFAS at the thin-water-film AWI on soil grain surfaces. Our framework combines the thermodynamics of interfacial adsorption and thin-water-film theory. Specifically, we couple an equation that describes the chemical equilibrium condition of PFAS with the Poisson-Boltzmann equation that governs the distribution of electrical potential in a thin water film. The end result is a mathematical model that can predict the

adsorption of PFAS at the thin-water-film AWI accounting for the interactions between the two EDLs of the AWI and the charged solid grain surface. We apply the model to study the anomalous PFAS adsorption at the thin-water-film AWI and analyze the primary factors that control the significance of the anomaly.

2. Mathematical Model for PFAS Adsorption at the Thin-Water-Film AWI

When air and water coexist in the pore space of soil, AWIs can arise from the thin water films covering soil grain surfaces and the pendular rings of water between soil grains (Figure 1a). The soil grain surfaces are often negatively charged (Sposito, 2016), attracting cations and repelling anions, which forms a so-called EDL that consists of two layers of charges: the first layer directly adheres to the surface and is referred to as the Stern layer (Stern, 1924), and the second layer is next to the Stern layer and is referred to as the diffuse layer. For bulk AWIs or AWIs of thin water films with greater thickness, the EDL associated with the soil grain surfaces and that of the AWI are far from each other with negligible interactions. However, when the thickness of the thin water films becomes smaller under drier conditions, the two EDLs can overlap (Figure 1b) and modify the electrical potential in the thin water film (Figure 1c). The modified electrical potential at the AWI will subsequently change the amount of adsorbed PFAS to reach a new chemical equilibrium condition. As a result, the adsorption at the thin-water-film AWI may deviate from that at the bulk AWI. In this section, we develop mathematical models to describe the potentially anomalous adsorption of PFAS at thin-water-film AWIs.

2.1. Chemical Equilibrium Among Thin-Water-Film and Bulk AWIs and Aqueous Solution

Assuming thermodynamic equilibrium at the pore scale (Figure 1) in a representative elementary volume of a porous medium, the chemical potentials of PFAS and counterion at the thin-water-film and bulk AWIs and the aqueous solution are equal

$$\mu_i^f = \mu_i^b = \mu_i^{aq}, \tag{1}$$

where μ is the chemical potential (J/mol). The superscripts f, b, and aq denote the thin-water-film AWI, bulk AWI, and aqueous solution, and the subscript i is either 1 or 2, denoting PFAS or counterion, respectively. We assume that the PFAS is fully dissociated in the aqueous solution due to their low concentrations in soil porewater at many contamination sites (Goss, 2008; Schaefer et al., 2022).

The chemical potential of PFAS and counterions in the aqueous solution is a function of their molar concentration c_i^{aq} and activity coefficient γ_i (e.g., Israelachvili, 2011)

$$\mu_i^{aq} = \mu_{0,i}^{aq} + RT \ln\gamma_i c_i^{aq}, \tag{2}$$

where $\mu_{0,i}^{aq}$ is the standard chemical potential of PFAS or counterion in the aqueous solution. The porewater of PFAS in the vadose zone can be considered a dilute solution, that is, the activity coefficient $\gamma_i \approx 1$. The standard chemical potential is defined as the chemical potential of a hypothetical ideal solution where the solute at a unit concentration (i.e., $c_i^{aq} = 1$/unit) (Prausnitz et al., 1998).

At the AWI, the chemical potential of adsorbed PFAS or counterion can be expressed as a function of the adsorption, $\widetilde{\Gamma}_i$ (mol/m^2). The adsorption $\widetilde{\Gamma}_i$ refers to the excess concentration of PFAS or counterion at the AWI. Following Kralchevsky et al. (1999), here we approximate $\widetilde{\Gamma}_i$ as the excess concentration in the Stern layer Γ_i because the excess concentration of PFAS in the diffuse layer is much smaller than that in the Stern layer. More details about the justification for this assumption and the description of the chemical potential for the adsorbed PFAS are presented in Supporting Information S1 (Text S1 and S2). For charged ionic PFAS, there is an additional contribution from the electrical potential to their chemical potential. A fraction of the ionic PFAS adsorbed at the AWIs may bind to the counterions. In that case, that fraction of adsorbed PFAS becomes electroneutral and their adsorption is not affected by the electrical potential. We denote the adsorption of PFAS at the thin-water-film AWI as Γ_1^f and that at the bulk AWI as Γ_1^b, respectively. Accordingly, the fraction of the adsorbed PFAS binding to counterions as β^f and β^b. The chemical potential of PFAS adsorbed at the thin-water-film and bulk AWIs can be written as

$$\mu_1^f = \mu_{0,1}^{\text{AWI}} + RT \ln\Gamma_1^f + \left(1 - \beta^f\right) v_1 F \psi^f, \tag{3}$$

$$\mu_1^b = \mu_{0,1}^{\text{AWI}} + RT \ln\Gamma_1^b + \left(1 - \beta^b\right) v_1 F \psi^b, \tag{4}$$

where $\mu_{0,1}^{\text{AWI}}$ is the standard chemical potential of the adsorbed PFAS at the AWIs, R is the universal gas constant (J/(mol K)), T is the temperature (K), v_1 is the valence of unbound PFAS, F is the Faraday constant (C/mol), and ψ^f is the electrical potential (V) at the thin-water-film AWI. The standard chemical potential of the adsorbed PFAS at the AWI can be defined as the chemical potential at unit adsorption (i.e., $\Gamma_1^f = 1$/units, $\Gamma_1^b = 1$/units) assuming there is no electrical potential at the AWI (i.e., $\psi^f = 0$, $\psi^b = 0$) (Prausnitz et al., 1998).

Assuming all adsorbed counterions bind to the adsorbed PFAS, if we let Γ_2^f and Γ_2^b be the adsorption of counterion at the thin-water-film and bulk AWIs, their chemical potential can be expressed as

$$\mu_2^f = \mu_{0,2}^{\text{AWI}} + RT \ln\Gamma_2^f, \tag{5}$$

$$\mu_2^b = \mu_{0,2}^{\text{AWI}} + RT \ln\Gamma_2^b, \tag{6}$$

where the standard chemical potential of counterion at the AWI, $\mu_{0,2}^{\text{AWI}}$, can be defined at unit adsorption (i.e., $\Gamma_2^f = 1$/units, $\Gamma_2^b = 1$/units).

The binding ratio at the thin-water-film AWI, β^f, and bulk AWI, β^b, is equal to the ratio between the adsorption of counterion and PFAS adsorbed at the AWI

$$\beta^f = \frac{\Gamma_2^f}{\Gamma_1^f}, \tag{7}$$

$$\beta^b = \frac{\Gamma_2^b}{\Gamma_1^b}. \tag{8}$$

Based on the thermodynamic equilibrium of PFAS between the thin-water-film and bulk AWIs presented above, we can derive a relationship between the adsorption of PFAS at the two types of AWIs, which is introduced in the following subsection.

2.2. Adsorption at the Thin-Water-Film AWI

To evaluate the anomalous adsorption, we determine PFAS adsorption at the thin-water-film AWI Γ_1^f for a given PFAS aqueous concentration c_1^{aq} and compare that to the adsorption at the bulk AWI Γ_1^b. To do so, we can relate Γ_1^f to Γ_1^b by equating the chemical potential at the thin-water-film and bulk AWIs. This is done by substituting Equations 3 and 4 to Equation 1

$$\Gamma_1^f = \Gamma_1^b \exp\left(\frac{v_1 F\left(\left(1 - \beta^b\right)\psi^b - \left(1 - \beta^f\right)\psi^f\right)}{RT}\right). \tag{9}$$

Equation 9 indicates that we can determine Γ_1^f if we obtain Γ_1^b, and the binding ratios β^f and β^b, and electrical potentials ψ^f and ψ^b at both AWIs.

PFAS adsorption at the bulk AWI, Γ_1^b, is a function of its aqueous concentration. Multiple adsorption isotherms can be used to model Γ_1^b, including the Langmuir-Szyszkowski isotherm discussed in Section 1 (e.g., Borwankar & Wasan, 1988; Davies, 1958; Kalinin & Radke, 1996; Kralchevsky et al., 1999). The standard Langmuir-Szyszkowski isotherm can only be used to compute the adsorption of surfactants at the bulk AWI for a given ionic strength when the surface tension data for that specific ionic strength are provided. Kralchevsky et al. (1999) generalized the Langmuir isotherm to explicitly account for the EDLs at the bulk AWI with also the capability to predict the surfactant adsorption at the bulk AWI for a wide range of ionic strength. We show that the adsorption

at the bulk AWI predicted by the generalized Langmuir isotherm of Kralchevsky et al. (1999) recovers that by the standard Langmuir-Szyszkowski isotherm for the range of environmentally relevant conditions examined in the present study (see Section S4 in Supporting Information S1). Here, we adopt the generalized Langmuir isotherm developed by Kralchevsky et al. (1999) and extend it to model PFAS adsorption at the AWI of thin water films.

The PFAS adsorption at the bulk AWI at a given aqueous concentration can be modeled as

$$\Gamma_1^b = \Gamma_m \frac{K c_1^{aq} \exp\left(-\frac{v_1 F \psi^b}{RT}\right)}{1 + K c_1^{aq} \exp\left(-\frac{v_1 F \psi^b}{RT}\right)}, \tag{10}$$

where Γ_m is the maximum air-water interfacial adsorption capacity (mol/m^2), and K is the adsorption coefficient for PFAS (m^3/mol) that can be computed as

$$K = K_1 + K_2 c_2^{aq} \exp\left(-\frac{v_2 F \psi^b}{RT}\right), \tag{11}$$

where K_1 (m^3/mol) and K_2 (m^6/mol^2) are two constants, and c_2^{aq} denotes the aqueous counterion concentration (mol/m^3).

The counterion adsorption at the bulk AWI Γ_2^b can be modeled by the counterion adsorption isotherm (Davies, 1958; Vassilieff et al., 1983)

$$\Gamma_2^b = \Gamma_1^b \frac{K_2/K_1 c_2^{aq} \exp\left(-\frac{v_2 F \psi^b}{RT}\right)}{1 + K_2/K_1 c_2^{aq} \exp\left(-\frac{v_2 F \psi^b}{RT}\right)}, \tag{12}$$

where K_2/K_1 is the counterion adsorption coefficient. According to the definition (i.e., $\beta^b = \Gamma_2^b/\Gamma_1^b$), the binding ratio at the bulk AWI β^b is the fractional part of the Equation 12

$$\beta^b = \frac{K_2 c_2^{aq} \exp\left(-\frac{v_2 F \psi^b}{RT}\right)}{K_1 + K_2 c_2^{aq} \exp\left(-\frac{v_2 F \psi^b}{RT}\right)}. \tag{13}$$

Note that instead of generalizing a Langmuir-type isotherm, the above theoretical development (Equations 10–13) can also be derived for other types of isotherms. Kralchevsky et al. (1999) presented a generalized Freundlich-type isotherm for surfactant adsorption at the bulk AWI. In the Supporting Information S1 (Text S3), we demonstrate that a Freundlich-type isotherm can also be adapted to describe PFAS adsorption at the AWI of thin water films.

Substituting Equations 5 and 6 into the chemical equilibrium of counterion (Equation 1), we obtain that the adsorption of counterion at the thin-water-film AWI Γ_2^f is equal to that at the bulk AWI Γ_2^b

$$\Gamma_2^f = \Gamma_2^b. \tag{14}$$

Therefore, the binding ratio at the thin-water-film AWI can be written as

$$\beta^f = \frac{\Gamma_2^b}{\Gamma_1^f}. \tag{15}$$

Because Γ_1^f in Equation 15 is an unknown, β^f can not be obtained directly. We compute β^f by solving the coupled Equation 15 and Equation 9.

The electrical potential at the thin-water-film AWI, ψ^f, and bulk AWI, ψ^b, can be obtained by solving the Poisson-Boltzmann equation, which describes the distribution of electrical potential caused by non-uniform ion

distribution. Assuming there are three types of ions (PFAS, counterion, and coion) in the solution and they possess a one-dimensional distribution perpendicular to the AWI in the thin water film or bulk water adjacent to the AWI, we employ a one-dimensional Poisson-Boltzmann equation

$$\frac{d^2\psi}{dz^2} = -\frac{F}{\varepsilon\varepsilon_0}\left(v_1 c_1^{aq}\exp\left(-\frac{v_1 F\psi}{RT}\right) + v_2 c_2^{aq}\exp\left(-\frac{v_2 F\psi}{RT}\right) + v_3 c_3^{aq}\exp\left(-\frac{v_3 F\psi}{RT}\right)\right),\qquad(16)$$

where ε is the relative dielectric constant (−) of water, ε_0 is the dielectric constant (C^2/J/m) of vacuum, and v_3 and c_3^{aq} are the valence and aqueous concentration of the coion.

For both the AWIs associated with the bulk water and the thin water film, two boundary conditions are required to solve Equation 16. For the bulk AWI, one boundary condition is at the AWI ($z = 0$) where the gradient of the electrical potential is related to the net charge of the adsorbed PFAS as

$$\left(\frac{d\psi}{dz}\right)_{z=0} = -\frac{\left(1-\beta^b\right)v_1 F\Gamma_1^b}{\varepsilon\varepsilon_0}.\qquad(17)$$

Assuming a semi-infinite domain, the other boundary condition is at infinity where the electrical potential gradient approaches zero

$$\left(\frac{d\psi}{dz}\right)_{z\to\infty} = 0.\qquad(18)$$

Solving Equation 16 subject to the two boundary conditions (Equations 17 and 18) gives the electrical potential at the bulk AWI ψ^b. Analytical solutions may be derived under certain conditions. For example, when the PFAS, counterion, and coion are univalent, an analytical solution can be derived for ψ^b based on the Gouy-Chapman theory (Verwey & Overbeek, 1955)

$$\psi^b = \frac{2RT}{F}\text{arc}\sinh\left(-\frac{\left(1-\beta^b\right)F\Gamma_1^b}{\sqrt{8\varepsilon\varepsilon_0 RTI}}\right),\qquad(19)$$

where I is the ionic strength of the solution (mol/m^3), which equals the counterion concentration (i.e., $I = c_2^{aq}$) for univalent PFAS, counterion, and coion. For more general conditions when ions with different charges are present, Equation 16 needs to be solved numerically.

For the thin water film, the boundary condition at the AWI is similar to that of the bulk AWI (Equation 17)

$$\left(\frac{d\psi}{dz}\right)_{z=0} = -\frac{\left(1-\beta^f\right)v_1 F\Gamma_1^f}{\varepsilon\varepsilon_0}.\qquad(20)$$

The other boundary condition is at the soil grain surface ($z = h$, h denotes the thickness of the thin water film) where the gradient of electrical potential is related to the charge density (C/m^2) of the soil grain surface ρ_s

$$\left(\frac{d\psi}{dz}\right)_{z=h} = -\frac{\rho_s}{\varepsilon\varepsilon_0}.\qquad(21)$$

The charge density ρ_s can be a function of PFAS adsorption at the soil grain surface. Because the soil grain surfaces are often negatively charged (Sposito, 2016), the adsorption of anionic PFAS at the soil grain surface may be considered negligible. In the present study, we assume that the ρ_s is a constant.

The electrical potential at the thin-water-film AWI, ψ^f, can be obtained by numerically solving Equation 16 subject to the two boundary conditions (Equations 20 and 21).

Equations 1–21 represent a mathematical model for determining the PFAS adsorption at the thin-water-film AWI for a given aqueous concentration. Three parameters need to be determined for solving these equations: K_1, K_2,

and Γ_m. These three parameters can be determined by fitting the equation of state at a bulk AWI to the measured surface tension as a function of PFAS aqueous concentration. For cases where PFAS, counterion, and coion are univalent, the equation of state (Equation 22) can be expressed as

$$\sigma = \sigma_0 - RT\Gamma_m \ln\left(1 + Kc_1^{aq} \exp\left(-\frac{v_1 F\psi^b}{RT}\right)\right) - \frac{4RT\sqrt{2\varepsilon_0\varepsilon_r RTI}}{F}\left(\cosh\left(\frac{F\psi^b}{2RT}\right) - 1\right), \quad (22)$$

where σ and σ_0 are the surface tension (N/m) with and without dissolved PFAS. More general forms of the equation of state at a bulk AWI for multivalent surfactants or swamping electrolyte ions are presented in Kralchevsky et al. (1999).

3. Numerical Solution

We present the numerical methods for solving the governing equations presented in Section 2 for PFAS adsorption at the thin-water-film AWI. The first step is to compute the PFAS adsorption Γ_1^b and binding ratio β^b as well as the electrical potential ψ^b at the bulk AWI by solving the coupled Equations 8, 10–12, and 16–18. After obtaining the variables for the bulk AWI, we then determine the PFAS adsorption Γ_1^f, binding ratio β^f, and the electrical potential ψ^f at the thin-water-film AWI, by solving Equations 9, 15, and 16 subject to the two boundary conditions (Equations 20 and 21). For convenience, hereafter we drop the subscript "1" and use Γ^b and Γ^f to denote PFAS adsorption at the bulk AWI and thin-water-film AWI, respectively.

The governing equations for the bulk and thin-water-film AWIs are both nonlinear and coupled, which we solve iteratively using the Newton-Raphson method. The key difference is how we solve the Poisson-Boltzmann equation (Equation 16). For bulk water, the Poisson-Boltzmann equation can be solved analytically under certain conditions. Here we assume that the PFAS, counterion, and coion are univalent and employ the analytical solution (Equation 19) of the Poisson-Boltzmann equation (Equation 16). For the thin water film, the Poisson-Boltzmann equation can only be solved numerically. We employ the finite difference method with a uniform grid ($\Delta z = 0.01$ nm) perpendicular to the thin water film. The second-order derivative is approximated by the central difference scheme. Because the boundary condition (Equation 20) of the Poisson-Boltzmann equation (Equation 16) is coupled with the PFAS adsorption at the thin-water-film AWI, we need to provide an initial guess for the adsorption and binding ratio at the AWI when solving the Poisson-Boltzmann equation for the electrical potential at the thin-water-film AWI. After that, we update the adsorption of PFAS using Equations 9 and 15. We repeat these two steps until the PFAS adsorption at the thin-water-film AWI converges.

4. Determination of Model Parameters

The mathematical model in Section 2 has three parameters, that is, K_1, K_2, and Γ_m, which we determine by fitting a surface equation of state at a bulk AWI (Equation 22) to the measured surface tension as a function of aqueous concentration for a specific PFAS. The present study selects a long-chain PFAS (i.e., PFOA) and a short-chain PFAS (i.e., PFHxA) as examples to illustrate the anomalous adsorption at the thin-water-film AWI. The surface tension data for these two PFAS were measured by the pendant drop method in NaCl solutions for five and four ionic strengths respectively, and were obtained from Le et al. (2021). Because the range of ionic strengths in Le et al. (2021) is higher than that in most soil porewater, we also include surface tension data for PFOA in NaCl solution at an ionic strength of 10 mM from Y. Lyu et al. (2018), which represents a typical ionic strength in soil porewater in the vadose zone. Note that Le et al. (2021) also reported the surface tension data for PFOA and PFHxA in deionized water. We did not use the deionized water surface tension data for the model fitting because the generalized Langmuir isotherm may not be applicable. The generalized Langmuir isotherm of Kralchevsky et al. (1999) relies on the assumption that the maximum adsorption capacity (Γ_m) remains constant for any salt concentrations, which may not be valid when there is no swamping electrolyte. No direct measurement of PFAS adsorption at the AWI at the maximum adsorption under different salt concentrations is available to verify this assumption, but such a data set (Tajima, 1970; Tajima et al., 1970) exists for a hydrocarbon surfactant (SDS). The maximum adsorption of SDS in NaCl solution of 115 mM measured by the radiotracer method (4.33 μmol/m^2) (Tajima, 1970) is 36% greater than that measured in deionized water (3.19 μmol/m^2) (Tajima et al., 1970).
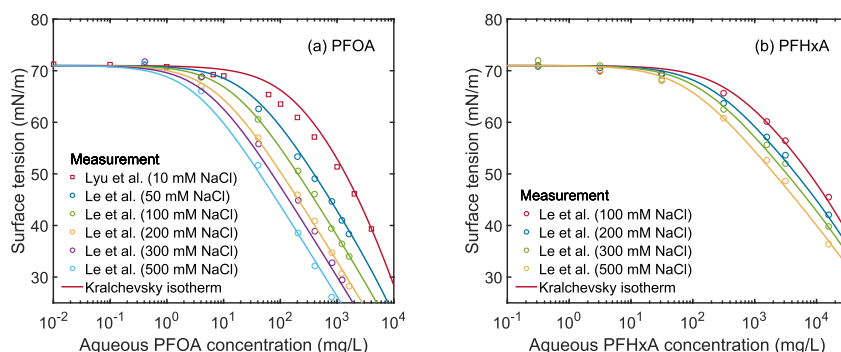
Figure 2. The fitting results of the surface tension data for (a) PFOA and (b) PFHxA under different ionic strengths, and the measurements for PFOA are from Le et al. (2021) (10 mM NaCl) and Le et al. (2021) (all other NaCl concentration) and that for PFHxA are from Le et al. (2021) only. The three fitting parameters K_1, K_2, and Γ_m are presented in Table 1.

We determine the three parameters K_1, K_2, and Γ_m by minimizing the mean square error of the modeled versus the measured surface tension. We do so by employing the interior-point method (Potra & Wright, 2000) via an iterative approach. For a given set of K_1, K_2, and Γ_m, because the adsorption isotherm (Equation 10), Gouy-Chapman model (Equation 19), and the equation of state (Equation 22) are coupled, we solve the three coupled equations to compute the surface tension. We observe that Equation 10 reduces to the standard Langmuir isotherm when $\psi^b \approx 0$, where the parameter K is equivalent to the standard Langmuir adsorption coefficient (K_L). This may be used as an additional constraint when estimating the model parameters. Based on this approximation, because K is a monotonic linear function of the aqueous counterion concentration, its intercept at $c_2^{aq} = 0$ (e.g., parameter K_1) should be smaller than the standard Langmuir adsorption coefficient at the lowest aqueous counterion concentration. For the surface tension data used in the present study, K_1 should be smaller than the K_L at the ionic strength of 10 mM for PFOA and 100 mM for PFHxA. The K_L can be determined by minimizing the mean squared error of the modeled versus the measured surface tension using the standard Langmuir-Szyszkowski model. The details about the standard Langmuir-Szyszkowski model are presented in the Supporting Information S1 (Section S4). We have incorporated the constraint of $K_1 < K_L$ when determining K_1, K_2, and Γ_m. We note that this additional constraint has a negligible impact on the analysis of the anomalous adsorption at the thin-water-film AWI. The anomaly of the adsorption at the thin-water-film AWI relative to that at the bulk AWI is only slightly greater when this additional constraint is not imposed.

The final modeled versus measured surface tensions are presented in Figure 2, which shows an excellent match for a wide range of PFAS concentrations and NaCl concentrations. Some slight discrepancy is observed for the case of PFOA in 10 mM NaCl. This may be caused by the surface tension data in the 10 mM NaCl solution case being obtained from a data set different from the other cases. The conditions under which the two data sets were obtained were slightly different, even though their overall conditions were the same. For example, the PFOA product used in Y. Lyu et al. (2018) has an impurity of 2%, while that used in Le et al. (2021) has an impurity of 4%. The uncertainties in the measured surface tension data due to small differences in different experiments (despite that they have the same overall conditions) are discussed in prior studies (e.g., Guo et al., 2023). The fitted parameters K_1, K_2, and Γ_m are summarized in Table 1. Four other constants used here and later in the paper are also included in Table 1. Finally, we point out that while we used PFOA and PFHxA in our examples, the model formulations and numerical framework also apply to other PFAS.

5. Results

We employ the mathematical model presented in Section 2 to study the adsorption of PFAS at the thin-water-film AWI and the primary factors that control its deviation from that at the bulk AWI. We first illustrate the anomalous adsorption of PFOA at the thin-water-film AWI using a base case with an ionic strength of 2 mM, a thickness of the thin water film of 6.8 nm,

Table 1
Determined Values for the Fitted Parameters K_1, K_2, and Γ_m for PFOA and PFHxA and Other Constants Used in the Simulations

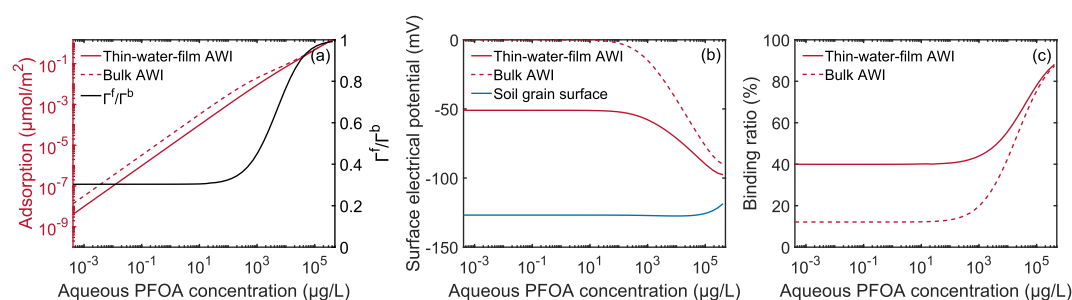| Parameter	PFOA	PFHxA	Unit
K_1	3.80	0.31	m^3/mol
K_2	0.26	0.0076	m^6/mol^2
Γ_m	3.12×10^{-6}	2.54×10^{-6}	mol/m^2
σ_0	71		dyn/cm
F	96,485		C/mol
ϵ_0	8.85×10^{-6}		C/J/m
ϵ_r	78.4		–

Figure 3. (a) Comparison between the computed adsorption of PFOA at thin-water-film and bulk air-water interfaces (AWIs). The ratio of Γ^f/Γ^b is also presented. (b) The electrical potential at the thin-water-film and bulk AWIs and soil grain surface. (c) The binding ratio at the thin-water-film and bulk AWIs. All the results are obtained for an ionic strength of 2 mM, a thickness of the thin water film of 6.8 nm, and a soil grain surface charge density of -30 mC/m^2.

and a soil grain surface charge density of -30 mC/m^2. We do so by comparing the computed adsorption at the thin-water-film AWI with that at the bulk AWI computed by the Kralchevsky et al. (1999) model. As mentioned earlier, the predicted adsorption at the bulk AWI by the Kralchevsky et al. (1999) model recovers the Langmuir-Szyszkowski model for the range of environmentally relevant conditions examined in the present study (Figure S3 in Supporting Information S1). Following the analyses of the base case, we conduct simulations covering a wide range of ionic strength, thickness of the thin water film, and soil grain surface charge density to investigate their impacts on anomalous adsorption at the thin-water-film AWI.

5.1. Illustration of the Anomalous Adsorption of PFAS at the Thin-Water-Film AWI

We illustrate the anomalous adsorption of PFAS at the thin-water-film AWI using the base case of PFOA as an example (Figure 3). The adsorption at the thin-water-film AWI approaches and eventually recovers that at the bulk AWI at higher aqueous concentrations, but the deviation increases as the concentration decreases (Figure 3a). Specifically, the ratio of the adsorption at the thin-water-film AWI and that at the bulk AWI, (i.e., Γ^f/Γ^b) is close to 1 for $c_{PFOA}^{aq} > 10^5$ µg/L, but decreases sharply as the PFOA concentration decreases (10^5 µg/L $> c_{PFOA}^{aq} > 10^2$ µg/L). Γ^f/Γ^b reaches a plateau at approximately 0.3 for $c_{PFOA}^{aq} < 10^2$ µg/L. For the base case, we have included PFAS aqueous concentrations greater than the environmentally relevant ranges in soil porewater to demonstrate that the adsorption at the thin-water-film AWI recovers that at the bulk AWI as the PFAS aqueous concentration increases (Figure 3a). In the rest of the paper, we only analyze the PFAS anomalous adsorption for concentrations lower than 5×10^3 µg/L to focus specifically on the environmentally relevant conditions.

The deviation of Γ^f from Γ^b is caused by the electrostatic interactions between the adsorbed PFAS at the thin-water-film AWI and the EDL of the soil grain surface (Section 2), which lead to the electrical potential and binding ratio at the thin-water-film AWI differing from that at a bulk AWI. Because the negatively charged PFAS in the aqueous solution is repelled from those adsorbed at the AWIs, a different electrical potential and a binding ratio at the AWI lead to a different amount of PFAS adsorption at the AWI. The reason Γ^f/Γ^b varies as a function of PFOA aqueous concentration is that the amount of negatively charged PFAS adsorbed at the AWI can change the relative importance of the impact from the EDL of the soil grain surface. At greater aqueous concentrations ($c_{PFOA}^{aq} > 10^2$ µg/L), a larger amount of adsorption generates a stronger EDL at the AWI, making the influence from the EDL of the soil grain surface smaller. This is demonstrated in Figure 3b where the electrical potential at the thin-water-film AWI approaches that at the bulk AWI at greater aqueous concentrations of PFOA. Consequently, the binding ratio at the thin-water-film AWI also approaches that at the bulk AWI at greater aqueous concentrations of PFOA (Figure 3c). At lower aqueous concentrations ($c_{PFOA}^{aq} < 10^2$ µg/L), the amount of adsorption decreases, leading to a weaker EDL at the AWI. The impact of the EDL of the soil grain surface becomes dominant, and the Γ^f/Γ^b decreases. The lower adsorption at the thin-water-film AWI leads to a greater binding ratio than that at the bulk AWI. However, the slightly increased binding ratio has a negligible impact on the adsorption—the binding ratio is approximately 40% and the remaining 60% PFAS are still negatively charged and are influenced by the EDL of the soil grain surface.

The analyses presented above indicate that the deviation is controlled by the competition between the EDLs of the thin-water-film AWI and soil grain surface. Γ^f deviates from Γ^b when the EDL of the soil grain surface dominates
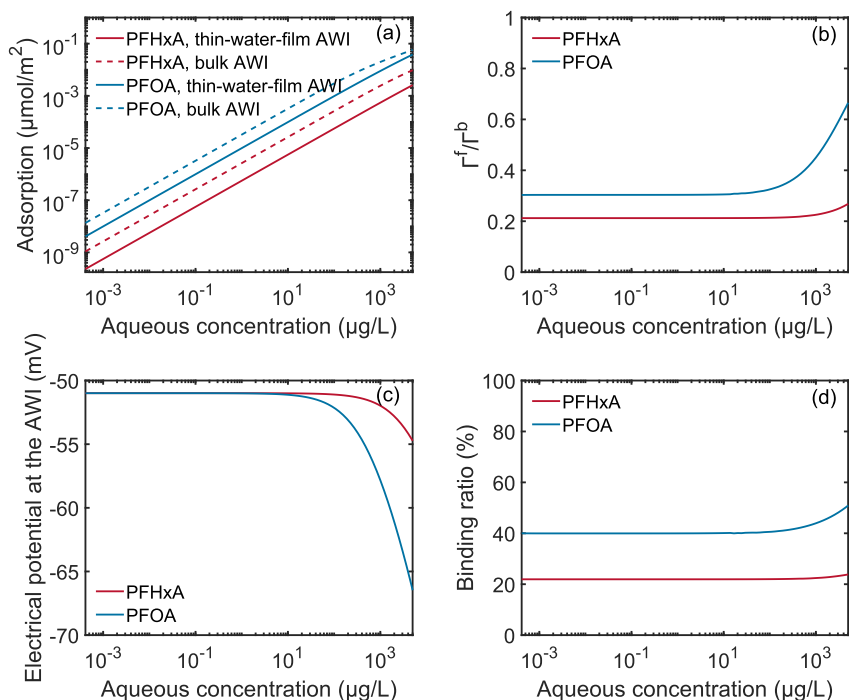
Figure 4. Impact of per- and poly-fluoroalkyl substances (PFAS) interfacial activity on the adsorption of PFAS at the thin-water-film air-water interfaces (AWIs) as a function of PFAS aqueous concentration: (a) The adsorption of PFAS at thin-water-film AWI versus that at the bulk AWI, (b) the ratio of Γ^f/Γ^b, and (c) the electrical potential and (d) the binding ratio at the thin-water-film AWI.

over that of the AWI. For a given surface charge density, the strength of the EDL of the soil grain surface remains unchanged. Because the EDL of the AWI becomes stronger at greater aqueous concentrations (greater adsorption) and weaker at smaller aqueous concentrations (smaller adsorption), the deviation is more pronounced at lower aqueous concentrations but smaller at higher concentrations.

5.2. Impact of PFAS Interfacial Activity

It is anticipated that the impact of the electrostatic interaction with the EDL of the soil grain surface will vary for different PFAS with different interfacial activities. For example, less interfacially-active PFAS will have lower adsorption for the same aqueous concentration, generating a weaker EDL at the AWI. Consequently, its adsorption at the AWI of a thin water film will be more greatly influenced by the EDL of the soil grain surface. Correspondingly, the adsorption of more interfacially-active PFAS will be less influenced by the EDL of the soil grain surface. We illustrate the impact of the interfacial activity on anomalous adsorption by comparing the results of the less interfacially-active PFHxA with PFOA for the base case.

The Γ^f for PFHxA exhibits similar deviation from Γ^b compared to that of PFOA (Figure 4b). There are two key differences: (a) the minimum Γ^f/Γ^b for PFHxA is 0.21 compared with 0.3 for PFOA; and (b) the Γ^f/Γ^b reaches the minimum at approximately $c_{\text{PFHxA}}^{aq} = 10^3$ μg/L for PFHxA, compared with approximately $c_{\text{PFOA}}^{aq} = 10^2$ μg/L for PFOA. The minimum Γ^f/Γ^b is smaller for PFHxA because PFHxA has a smaller binding ratio (22%) than PFOA (40%) (Figure 4d) while the electrical potentials at the AWI are the same (Figure 4c) at lower concentrations. As a result, a greater fraction of the adsorbed PFHxA is impacted by the EDL of the soil grain than that of PFOA. The Γ^f/Γ^b for PFHxA reaches the minimum at a greater aqueous concentration because the adsorption of PFHxA is much lower (approximately two orders of magnitude) than PFOA for the same aqueous concentration (Figure 4a). The lower adsorption leads to a smaller charge density at the AWI, requiring a concentration two orders of magnitude higher for PFHxA to achieve the same strength in the EDL of the AWI as that for PFOA. This can also be seen from the fact that a much larger aqueous concentration is needed for PFHxA to reach the same electrical potential at the AWI as that of PFOA (Figure 4c).
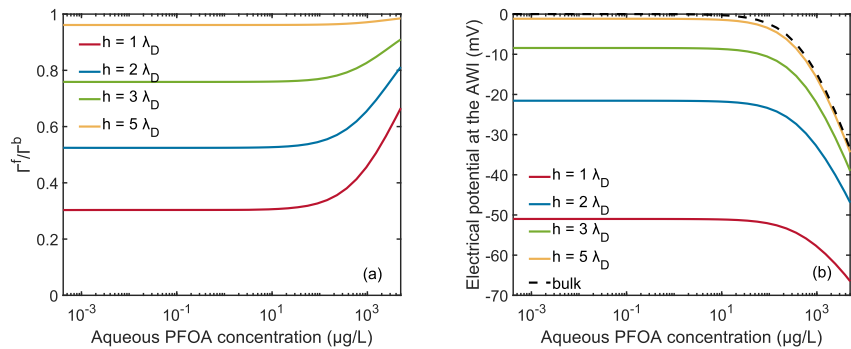
Figure 5. Impact of the thickness of the thin water film on the adsorption of PFOA at the thin-water-film air-water interface (AWI): (a) the ratio between the adsorption at the thin-water-film and bulk AWIs and (b) the electrical potential at the AWIs.

5.3. Impact of the Thickness of the Thin Water Film

The thickness of the thin water film controls the extent of the overlap between the EDLs of the soil grain surface and AWI (Section 2). In a thin water film with a greater thickness, the two EDLs are further from each other, and the EDL of the soil grain surface has a smaller impact on the PFAS adsorption at the AWI. We conduct simulations using the base case for PFOA with a range of thicknesses of the thin water film to examine this impact and identify the critical thickness of the thin water film beyond which the adsorption anomaly at the AWI of a thin water film vanishes.

In water-unsaturated soil media, the thickness of thin water films is a function of the ionic strength of porewater, the charge density of the soil grain surface, and the matrix potential (Nishiyama & Yokoyama, 2021; Tokunaga, 2011). The charge density of the soil grain surface and the ionic strength are fixed in this subsection. We normalize the thin water film thickness by the Debye length (λ_D)—the distance at which the electrical potential drops to $1/e$ of that at the interface (Debye & Hückel, 1923). The Debye length can be computed as

$$\lambda_D = \sqrt{\frac{\varepsilon_0 \varepsilon_r RT}{2F^2 I}}. \tag{23}$$

The normalized thickness represents the relative thickness of the thin water film compared to that of the EDL. We consider the following thicknesses for the thin water film $h = \lambda_D$, $h = 2\lambda_D$, $h = 3\lambda_D$, and $h = 5\lambda_D$. For the base case ionic strength (2 mM), the corresponding absolute thicknesses of the thin water film are 6.8, 13.6, 20.4, and 34 nm, respectively.
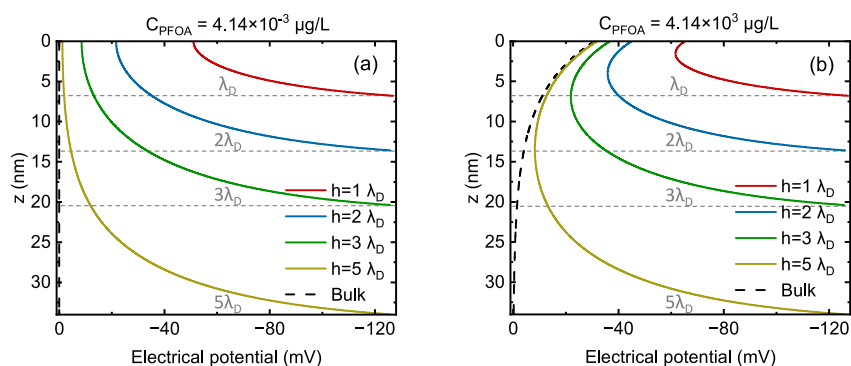

Figure 6. Comparison of electrical potential profiles away from the air-water interface (AWI) ($z = 0$) for different thicknesses of the thin water film at two different PFOA aqueous concentrations: (a) $c_{PFOA}^{aq} = 4.14 \times 10^{-3}$ μg/L and (b) $c_{PFOA}^{aq} = 4.14 \times 10^{3}$ μg/L. The gray dash lines indicate the position of the soil grain surface for the thin water films with different thicknesses.
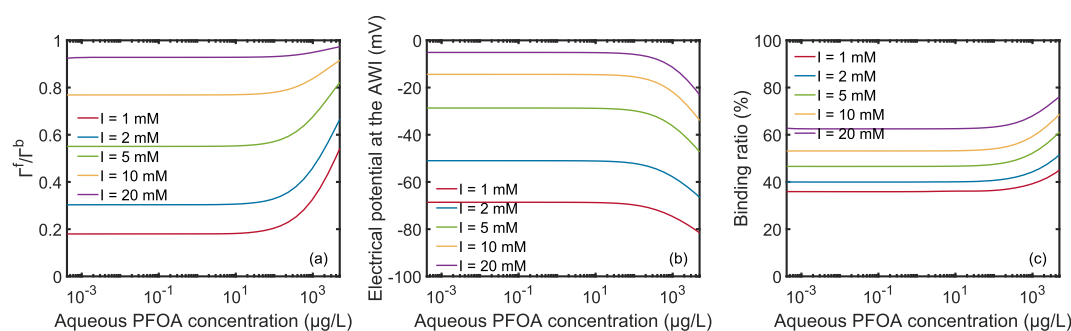
Figure 7. Impact of the ionic strength on the adsorption of PFOA at the thin-water-film air-water interface (AWI) as a function of PFOA aqueous concentration: (a) the ratio between the adsorption at the thin-water-film and bulk AWIs, (b) the electrical potential and (c) the binding ratio at the thin-water-film AWI.

Inspection of Figure 5a reveals that Γ^f deviates more from Γ^b as the thickness of the thin water film becomes smaller. At lower PFOA concentrations where the deviation reaches the maximum, Γ^f/Γ^b is approximately 0.96, 0.76, 0.52, and 0.3 for $h = 5\lambda_D$, $h = 3\lambda_D$, $h = 2\lambda_D$, and $h = \lambda_D$, respectively. The reduced deviation for a thin water film with a greater thickness results from a smaller impact from the EDL of the soil grain surface. As illustrated in Figure 5b, the electrical potential becomes less negative as the thickness of the thin water film increases and eventually almost recovers that at the bulk AWI for $h = 5\lambda_D$.

The more negative electrical potential observed at the AWI for a smaller h is caused by the stronger interactions between the EDLs of the soil grain surface and AWI. This is illustrated in Figure 6a for a lower PFOA concentration ($c_{PFOA}^{aq} = 4.14 \times 10^{-3}$ µg/L), where the electrical potential in the thin water film becomes more negative as the thickness of the thin water film decreases. At $h = 5\lambda_D$, the electrical potential at the AWI of the thin water film almost recovers that at the bulk AWI, indicating minimal impact on the AWI from the overlapping of the EDLs. For a much greater PFOA aqueous concentration ($c_{PFOA}^{aq} = 4.14 \times 10^3$ µg/L) (Figure 6b), the EDL of the thin-water-film AWI becomes much stronger. The electrical potential at the AWI is still more negative as the thickness of the thin water film decreases, but the change is much smaller relative to the case of a smaller PFOA concentration. This explains why the deviation of the thin-water-film adsorption becomes smaller as the PFOA aqueous concentration increases—the relative impact from the EDL of the soil grain surface decreases as the EDL of the AWI becomes stronger.

5.4. Impact of the Ionic Strength

It is well known that the EDLs are a function of the ionic strength of an aqueous solution. More free ions in a solution with a higher ionic strength reduce the Colombian interaction range, that is, the so-called electrostatic screening effect. This effect reduces the thickness of both the EDLs of the AWI and soil grain surface. Furthermore, at a higher ionic strength, the adsorbed PFAS at the AWI is more likely to bind to counterions and become neutral, which leads to a smaller fraction of the adsorbed PFAS affected by the EDL of the solid surface. Thus, we hypothesize that the anomalous adsorption at the AWI of a thin water film will also depend on the ionic strength. To test this hypothesis, we take the base case of PFOA as an example and consider a range of ionic strength from 1 to 20 mM while fixing the charge density of the soil grain and the water film thickness.

The results show that Γ^f deviates more from Γ^b at a lower ionic strength (Figure 7a). At lower PFOA concentrations where the deviation reaches the maximum, Γ^f/Γ^b is approximately 0.92 and 0.18 for $I = 20$ mM and $I = 1$ mM, respectively. The greater deviation observed at a lower ionic strength is due to both a lower binding ratio (Figure 7c) and a stronger impact from the interactions between the EDLs of the AWI and soil grain surface. The lower binding ratio results from fewer free counterions at a lower ionic strength. The interactions between the EDLs of the AWI and soil grain surface are stronger due to their increased thickness at a lower ionic (i.e., weaker electrostatic screening effect). This is also reflected in the more negative electrical

Table 2
The Debye Length and Normalized Water Film Thickness for Different Ionic Strengths

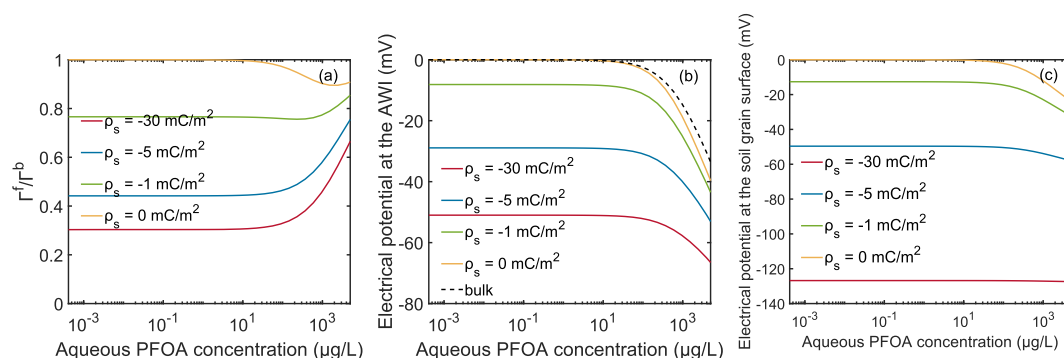| Ionic strength, I (mM)	Debye length, λ_D (nm)	Normalized water film thickness, h/λ_D
1	9.6	0.7
2	6.8	1
5	4.3	1.6
10	3.0	2.3
20	2.2	3.1

Figure 8. Impact of soil grain surface charge density on the adsorption of PFOA at the thin-water-film air-water interface (AWI): (a) the ratio between the adsorption at the thin-water-film and bulk AWIs, and the electrical potential (b) at the AWIs and (c) at the soil grain surface.

potential at the AWI of the thin water film as the ionic strength decreases (Figure 7b).

For the system we analyze, the Debye length λ_D increases from 2.2 nm at $I = 20$ mM to 9.6 nm at $I = 1$ mM (Table 2). For the fixed thickness of the thin water film ($h = 6.8$ nm), the normalized water film thickness decreases from 3.1 at $I = 20$ mM to 0.7 at $I = 1$ mM (Table 2). It is interesting to note that even though the thickness of the thin water film is more than three times the Debye length at $I = 20$ mM, we still observe 7% deviation of Γ^f from Γ^b resulting from the electrostatic interaction between the EDL of the soil grain surface and the PFOA adsorbed at the thin-water-film AWI.

To demonstrate that the normalized thickness of the thin water film is not the only factor controlling Γ^f/Γ^b, we compare the case of $I = 20$ mM ($h = 3.1\lambda_D$) with the case of $h = 3\lambda_D$ ($I = 2$ mM) presented in Section 5.3. These two cases have almost the same normalized water film thickness, but the minimum Γ^f/Γ^b is 0.76 for the case of $h = 3\lambda_D$ in Section 5.3, which is smaller than the case of $h = 3.1\lambda_D$ analyzed here ($\Gamma^f/\Gamma^b = 0.92$). A closer inspection reveals that the case of $h = 3\lambda_D$ in Section 5.3 has a smaller binding ratio (approximately 16% at lower PFOA aqueous concentrations) due to the much lower ionic strength ($I = 2$ mM). As a result, a greater fraction of the PFOA adsorbed at the AWI is charged and affected by the EDL of the soil grain surface, which subsequently leads to a greater deviation of Γ^f from Γ^b.

5.5. Impact of the Charge Density of the Soil Grain

In the vadose zone, the surface charge of soil grain surfaces may vary for different minerals and under different conditions (Kumari & Mohan, 2021; Sposito, 2016). The chemistry of porewater, such as pH, may modify the surface charge (Kretzschmar et al., 1998). Typically, the charge density of negatively charged mineral surfaces in the soil can range from 0 to -30 mC/m^2 (Guo & Yu, 2017; Kroutil et al., 2015). Soil grains with a higher (i.e., more negative) surface charge generate a stronger EDL at the soil grain surface. Subsequently, this can lead to a greater deviation of Γ^f from Γ^b. We quantify the impact of surface charge density on PFAS adsorption at the thin-water-film AWI using the base case for PFOA under different charge densities.

Figure 8a shows that a greater surface charge density leads to a smaller ratio of Γ^f/Γ^b, suggesting a greater deviation of Γ^f. When the deviation reaches the maximum at lower concentrations, Γ^f/Γ^b is approximately 0.3, 0.44, and 0.77 for charge densities of -30, -5, and -1 mC/m^2, respectively (Figure 8a). It is interesting that Γ^f/Γ^b is below 1 even for the electrically neutral soil grain surface ($\rho_s = 0$) over some range of aqueous PFOA concentration ($c_{PFOA}^{aq} > 10$ μg/L). This is because the EDL at the AWI is not fully developed in a thin water film with a thickness of 6.8 nm.

The surface charge density influences PFAS adsorption because a greater surface charge density leads to a stronger EDL at the soil grain surface, as indicated by the greater electrical potential at the soil grain surface (Figure 8c). Consequently, the magnitude of the electrical potential at the AWI increases (i.e., becomes more negative) (Figure 8b), rising from 8 to 51 mV at lower PFOA aqueous concentrations as the charge density changes from $\rho_s = -1$ mC/m^2 to $\rho_s = -30$ mC/m^2. The modified electrical potential directly changes the chemical potential of the negatively charged PFAS at the thin-water-film AWI and the overall PFAS adsorption.

6. Discussion

We have developed a mathematical model that describes the adsorption of PFAS at the thin-water-film AWI. The model accounts for the interaction between the EDLs of the soil grain surface and the thin-water-film AWI, and the subsequent impact on the adsorption of PFAS at the thin-water-film AWI. This is done by coupling the chemical equilibrium condition of PFAS interfacial adsorption to the Poisson-Boltzmann equation that describes the distribution of electrical potential in a thin water film. The mathematical model has three parameters, which can be determined by fitting a surface equation of state to the measured surface tension data at different ionic strengths for a specific PFAS. The new mathematical model allows us to examine the potentially anomalous adsorption of PFAS at the thin-water-film AWI. Our analyses suggest that PFAS adsorption at the AWI of a thin water film sitting on soil grain surfaces can deviate significantly from that at a bulk AWI. The deviation results from the overlap of the EDLs of the soil grain surface and that of the thin-water-film AWI. The extent of the deviation is a function of several parameters, including the interfacial activity of the PFAS, porewater ionic strength, the thickness of the thin water film, and soil grain surface charge. Specifically, lower porewater ionic strength, smaller thickness of the thin water film, and greater soil grain surface charge density all amplify the overlap of the two EDLs and lead to a greater deviation of Γ^f from Γ^b. Finally, while the present study has only illustrated the anomalous PFAS adsorption at the thin-water-film AWI when the adsorbed PFAS and the soil grain surface have the same charge sign, the theoretical framework can be generalized to account for other conditions, such as when the adsorbed PFAS and the soil grain surface have opposite charge signs.

6.1. Regime Diagram for the Anomalous Adsorption of PFAS at Thin-Water-Film AWIs in the Vadose Zone

Building upon the analyses in Section 5, here we comment on the conditions under which the anomalous adsorption at thin-water-film AWIs is significant in the vadose zone at PFAS contamination sites. The PFAS porewater concentrations at many legacy PFAS contamination sites are relatively low. For example, recent soil porewater sampling and analysis (Anderson et al., 2022; Brusseau & Guo, 2022; Quinnan et al., 2021; Schaefer et al., 2022) at multiple AFFF-impacted contamination sites suggest that the porewater concentration of PFOA is always below 4.9×10^3 µg/L. Similar porewater concentrations were observed for other types of PFAS at AFFF-impacted contamination sites. The maximum porewater concentrations are approximately 5.7×10^3 µg/L for PFHxA, 8×10^3 µg/L for PFOS, and 2×10^4 µg/L for PFHxS. Because AFFF-impacted sites are among the most highly contaminated sites, the porewater concentrations at non-AFFF sites, including biosolids-impacted agricultural lands, and contamination sites related to wastewater treatment plants and landfills, are likely much lower. These concentration ranges and the analyses in Section 5 suggest that the porewater at most PFAS contamination sites will be in the lower aqueous concentration region where the deviation of Γ^f from Γ^b reaches the maximum.

At the maximum deviation of Γ^f from Γ^b at the lower concentrations, we compute the ratio of Γ^f/Γ^b for different normalized thicknesses of the thin water film and soil grain surface charge densities and then generate a 2D heat map (Figure 9a). The color denotes the ratio of Γ^f/Γ^b. The heat map clearly shows that a smaller thickness of the thin water film (normalized by the Debye length) and a greater charge density (i.e., more negative) increase the deviation (i.e., Γ^f/Γ^b is smaller). Given that the experimental uncertainty for the bulk air-water interfacial adsorption coefficient $\left(K_{aw}^b = \Gamma^b/c_1^{aq}\right)$ was reported to be approximately 25% (e.g., Brusseau & Guo, 2021), we use 25% as the threshold to define the anomalous adsorption of PFAS at the thin-water-film AWIs. With this threshold, the combination of the thickness of the thin water film and the surface charge density outside of the equivalue curve of $\Gamma^f/\Gamma^b = 0.75$ (Figure 9a) may be considered to have a negligible anomaly in the adsorption of PFAS at the thin-water-film AWI.

The thickness of the thin water film on soil grain surfaces is a function of the matric potential, porewater ionic strength, and surface charge density in the soil media. For two limiting ionic strength values (1 and 100 mM) in the vadose zone, we compute the thickness of the thin water film following Tokunaga (2011) for the range of commonly observed matric potential (from −500 to 0 cm) and surface charge density (from −30 to 0 mC/m^2) in the vadose zone, which generates two surfaces in Figure 9b (the blue surfaces). The details about how to compute the thickness of the thin water film under different matric potentials and soil grain surface charge densities are presented in Supporting Information S1 (Text S5). The thickness of the thin water film within these two surfaces can be considered as the range commonly observed in the vadose zone. For a given matrix potential and an ionic
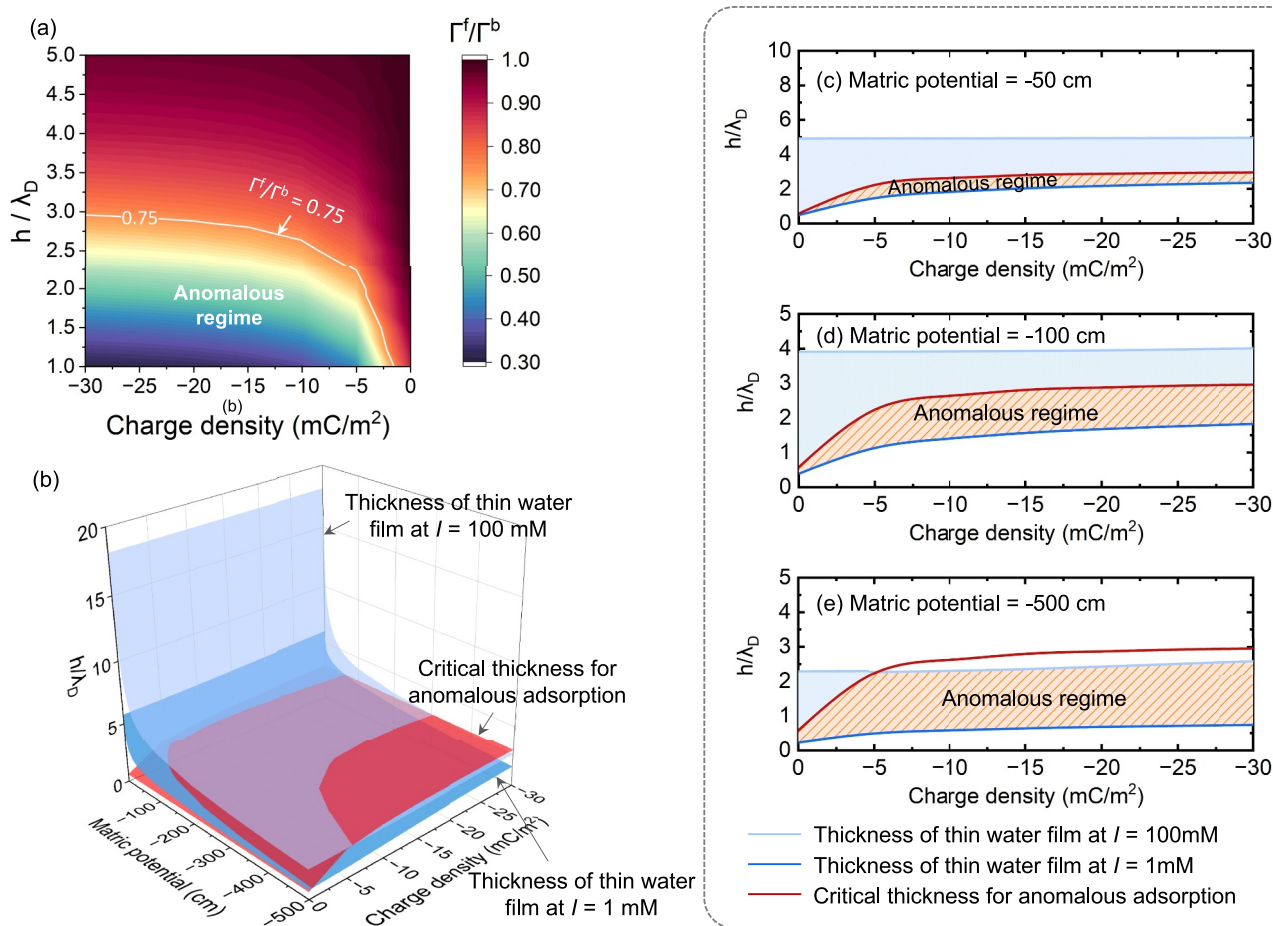
Figure 9. (a) The ratio of Γ^f/Γ^b at the lower PFOA aqueous concentrations with various charge densities and dimensionless thicknesses of the thin water film. The white curve represents the threshold for the anomalous adsorption of the thin-water-film air-water interface. The heat map is obtained with a grid resolution of 0.5 h/λ_D and 5 mC/m². (b) The critical thickness of the thin water film versus matric potential and soil grain charge density compared with the dimensionless thickness of the thin water film in the vadose zone. The cross-section view of (b) at matric potentials of (c) −50 cm, (d) −100 cm, and (e) −500 cm. The orange stripe area denotes the anomalous regime while the light blue area denotes the normal regime.

strength, we can then determine the critical thickness of the thin water film below which $\Gamma^f/\Gamma^b < 75\%$, where the anomalous adsorption is important and may need to be considered. This gives a third surface in Figure 9b (the red surface). The regime falling within the intersection of the three surfaces represents the anomalous regime where the deviation of the adsorption at the thin-water-film AWI from that at the bulk AWI needs to be considered. To illustrate the anomalous regime, we plot 2D cross-sections at three matrix potential values of −50, −100, and −500 cm (Figure 9c–9e). The results show that anomalous adsorption is less likely in wetter soil (i.e., greater matrix potential) and for smaller grain surface charge density. However, anomalous adsorption occurs under a wide range of conditions (represented by the matrix potential, porewater ionic strength, and soil grain surface charge density) in the vadose zones as indicated by the stripe area in Figures 9c–9e.

While our mathematical model and analyses have considered a variety of processes, there are a few potentially important factors that have not been accounted for in our study. These include the pH and the presence of counterions with different valences in the porewater, and PFAS mixtures especially those with the opposite charge signs. The porewater pH can modify the binding ratio of the adsorbed PFAS. Porewater with a lower pH has more free protons that can bind to negatively charged PFAS at the AWI. This will increase the fraction of non-charged PFAS at the AWI and subsequently reduce the impact from the EDL of the soil grain surface, which may reduce the deviation of Γ^f from Γ^b. The impact of pH may be accounted for by treating the proton as another counterion. Because this is the first analysis being done for PFAS interfacial adsorption at the AWI of thin water
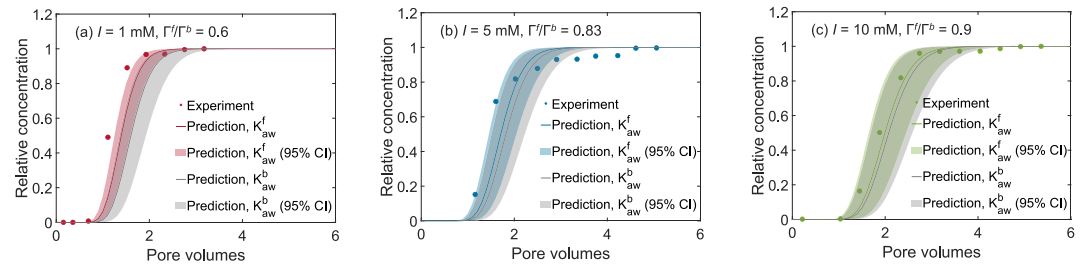
Figure 10. Comparisons between the predicted and measured breakthrough curves of PFOA in a water-unsaturated sand-packed column at water saturation of 0.68 with different ionic strengths: (a) $I = 1$ mM, (b) $I = 5$ mM, and (c) $I = 10$ mM. The colored lines and gray lines are the simulation results with and without accounting for the anomalous adsorption, respectively. The shaded area represents the model simulation using 95% confidence interval values for the air-water interfacial adsorption coefficient and air-water interfacial area. The measured breakthrough curves are obtained from Y. Lyu and Brusseau (2020).

films, we have considered the simpler case of PFAS and counterion having the same valence. At PFAS contamination sites, soil porewater in the vadose zone could have different types of salts with counterions or coions of different valences, such as Na^+, Ca^{2+}, or Mg^{2+}. When counterions with different valences are co-present, their binding with PFAS at the AWI can be more involved, for example, two univalent PFAS may be bound to one Ca^{2+} or Mg^{2+}. The model formulations developed in the present study need to be extended to account for these effects. Finally, we have selected two example PFAS—PFOA and PFHxA for demonstration purposes. As more surface tension data sets become available in the future, the modeling framework can be extended to analyze more complicated conditions as well as for a broader range of PFAS that are of practical interest.

6.2. Impact of the Anomalous Adsorption on PFAS Transport in Water-Unsaturated Porous Media

The anomalous adsorption of PFAS at the thin-water-film AWI may reduce the retention of anionic PFAS (or increase the retention of cationic PFAS) in the vadose zone and subsequently increase (or decrease in the case of cationic PFAS) the mass discharge to groundwater. We have compiled the available miscible-displacement experimental data for PFOA (conducted in packed columns of quartz sand, glass beads, or limestone) from a total of seven studies in the literature (Brusseau & Guo, 2021; Brusseau et al., 2019; Li et al., 2021; Y. Lyu & Brusseau, 2020; Y. Lyu et al., 2018, 2020, 2022), and computed the ratio of Γ^f/Γ^b in these experiments. The computed Γ^f/Γ^b are summarized in Table S5 in Supporting Information S1. Because all of these miscible-displacement experiments were conducted at a large (i.e., less negative) matric potential, the anomaly of adsorption is insignificant for most cases except for that in the study of Y. Lyu and Brusseau (2020). To further demonstrate the impact of the anomalous adsorption on PFOA transport in the water-unsaturated porous media, we have incorporated our adsorption isotherm for the thin-water-film AWI to the PFAS transport model presented in Guo et al. (2020). We then simulated the miscible-displacement experiment with the greatest anomaly (Y. Lyu & Brusseau, 2020) and compared the model simulations (using adsorption isotherm for both thin-water-film and bulk AWIs) with the experimental measurement of the breakthrough curve. To account for uncertainties in the model parameters, we have also conducted simulations using the lower and upper 95% confidence interval of the two critical parameters: the air-water interfacial adsorption coefficient (K^f_{aw} or K^b_{aw}) and the air-water interfacial area (A_{aw}). The air-water interfacial adsorption coefficient at the thin-water-film AWI, K^f_{aw}, is defined as the ratio between the amount of adsorption at the thin-water-film AWI and the aqueous concentration (i.e., $K^f_{aw} = \Gamma^f/c^{aq}_1$). All of the input parameters are determined a priori, thus the model simulations represent independent predictions. A summary of the compiled data from the seven studies and additional details of the model simulations and analyses of the miscible-displacement studies are presented in Supporting Information S1 (Text S6 and S7).

The results show that the predicted breakthrough curve (Figures 10b and 10c) and computed retardation factor (Table S7 in Supporting Information S1) using the adsorption isotherm at the thin-water-film AWI match well with the measurement for the cases of $I = 5$ mM and $I = 10$ mM (within the 95% confidence interval). For the case of $I = 1$ mM, the model prediction overestimates the retention, but the predicted breakthrough curve using the lower 95% confidence interval values of K^f_{aw} and A_{aw} is still close to the measurement (Figure 10a). For all three

cases, the model predictions using the adsorption isotherm at the bulk AWI lead to stronger retention and subsequently deviate from the measurement, though the measured breakthrough curve still falls within the 95% confidence interval of the model predictions for the cases of $I = 5$ mM and $I = 10$ mM. For the case of $I = 1$ mM, the measured breakthrough curve deviates further from the model prediction, compared to that using the adsorption isotherm at the thin-water-film AWI.

While the model predictions using the adsorption isotherm at the thin-water-film AWI have a better agreement with the measurement than that using the adsorption isotherm at the bulk AWI, we are cautious of concluding that the comparisons indicate the impact of anomalous adsorption at the thin-water-film AWI. This is because the anomaly of adsorption under these specific experimental conditions is not sufficiently large to isolate the impact of experimental uncertainties. To better differentiate the anomalous adsorption at the thin-water-film AWI from that at the bulk AWI, additional experiments should be conducted using smaller matric potential (i.e., either by using a lower water saturation or by using finer-grain porous media) or lower ionic strengths where the anomalous adsorption becomes more significant. Finally, we note while the matric potential is quite large (-30.9 to -14.5 cm) for the water saturation ranging from 0.35 to 0.87 in the reported miscible-displacement experiments that used idealized porous media (Table S5 in Supporting Information S1), the matric potential can be much smaller (i.e., much more negative) in the vadose zone under field conditions. The typical matric potential under field conditions can go down to -300 cm or lower (e.g., Singh et al., 2018), where the anomaly of adsorption at the thin-water-film AWI is expected to be much stronger. The specific impact of the anomalous adsorption of PFAS at the thin-water-film AWI on PFAS leaching in the vadose zone under field conditions needs to be evaluated in future studies.

7. Conclusion

We have developed a mathematical model for PFAS adsorption at the thin-water-film AWI. The model formulation couples the chemical equilibrium condition of PFAS interfacial adsorption with the Poisson-Boltzmann equation. The model has three parameters, which can be determined by fitting a surface equation of state to measured surface tension data covering different ionic strengths. We have applied the model to analyze the deviation of Γ^f from Γ^b under a wide range of conditions relevant to water-unsaturated soils in the vadose zone at PFAS contamination sites. Using PFOA and PFHxA as examples, we illustrate that the anomalous adsorption at thin-water-film AWI is controlled by several primary factors, including PFAS interfacial activity, ionic strength, thickness of the thin water film, and soil grain charge density.

The model simulations and analyses suggest that the adsorption of PFAS at the thin-water-film AWI can strongly deviate from that at bulk AWIs under many conditions in the vadose zone. The anomaly of adsorption increases as the PFAS aqueous concentration decreases and is particularly prominent at PFAS porewater concentrations commonly encountered in many legacy PFAS contamination sites. Under conditions relevant to the vadose zone of PFAS contamination sites, the deviation of Γ^f from Γ^b can be up to 82% for the scenarios considered in the present study. Our findings underscore the importance of considering the impact of thin water films on PFAS adsorption at the AWI when studying the fate and transport of PFAS in the vadose zone.

Data Availability Statement

All the datasets used in the present study, including the surface tension data, are from the literature and are included in the manuscript and its supporting information, tables, and/or figures. The model simulation output used to generate the figures in the paper and its supplementary files (Zhang & Guo, 2023) is available at https://doi.org/10.5281/zenodo.10086205.

References

Adamson, A. W., & Gast, A. P. (1997). Physical chemistry of surfaces (6th ed., Vol, 720). Wiley.

Adamson, D. T., Nickerson, A., Kulkarni, P. R., Higgins, C. P., Popovic, J., Field, J., et al. (2020). Mass-based, field-scale demonstration of PFAS retention within AFFF-associated source areas. *Environmental Science & Technology*, *54*(24), 15768–15777. https://doi.org/10.1021/acs.est.0c04472

An, S., Lu, J., Thomas, R., & Penfold, J. (1996). Apparent anomalies in surface excesses determined from neutron reflection and the Gibbs equation in anionic surfactants with particular reference to perfluorooctanoates at the air/water interface. *Langmuir*, *12*(10), 2446–2453. https://doi.org/10.1021/la950851y

Anderson, R. H., Adamson, D. T., & Stroo, H. F. (2019). Partitioning of poly-and perfluoroalkyl substances from soil to groundwater within aqueous film-forming foam source zones. *Journal of Contaminant Hydrology*, *220*, 59–65. https://doi.org/10.1016/j.jconhyd.2018.11.011

Anderson, R. H., Feild, J. B., Dieffenbach-Carle, H., Elsharnouby, O., & Krebs, R. K. (2022). Assessment of PFAS in collocated soil and porewater samples at an AFFF-impacted source zone: Field-scale validation of suction lysimeters. *Chemosphere*, *308*, 136247. https://doi.org/10.1016/j.chemosphere.2022.136247

Aveyard, B. (2019). *Surfactants: In solution, at interfaces and in colloidal dispersions*. Oxford University Press.

Borwankar, R., & Wasan, D. (1988). Equilibrium and dynamics of adsorption of surfactants at fluid-fluid interfaces. *Chemical Engineering Science*, *43*(6), 1323–1337. https://doi.org/10.1016/0009-2509(88)85106-6

Braun, L., Uhlig, M., von Klitzing, R., & Campbell, R. A. (2017). Polymers and surfactants at fluid interfaces studied with specular neutron reflectometry. *Advances in Colloid and Interface Science*, *247*, 130–148. https://doi.org/10.1016/j.cis.2017.07.005

Brusseau, M. L. (2021). Examining the robustness and concentration dependency of PFAS air-water and NAPL-water interfacial adsorption coefficients. *Water Research*, *190*, 116778. https://doi.org/10.1016/j.watres.2020.116778

Brusseau, M. L., & Guo, B. (2021). Air-water interfacial areas relevant for transport of per and poly-fluoroalkyl substances. *Water Research*, *207*, 117785. https://doi.org/10.1016/j.watres.2021.117785

Brusseau, M. L., & Guo, B. (2022). PFAS concentrations in soil versus soil porewater: Mass distributions and the impact of adsorption at air-water interfaces. *Chemosphere*, *302*, 134938. https://doi.org/10.1016/j.chemosphere.2022.134938

Brusseau, M. L., Anderson, R. H., & Guo, B. (2020). PFAS concentrations in soils: Background levels versus contaminated sites. *Science of the Total Environment*, *740*, 140017. https://doi.org/10.1016/j.scitotenv.2020.140017

Brusseau, M. L., Guo, B., Huang, D., Yan, N., & Lyu, Y. (2021). Ideal versus nonideal transport of PFAS in unsaturated porous media. *Water Research*, *202*, 117405. https://doi.org/10.1016/j.watres.2021.117405

Brusseau, M. L., Peng, S., Schnaar, G., & Costanza-Robinson, M. S. (2006). Relationships among air–water interfacial area, capillary pressure, and water saturation for a sandy porous medium. *Water Resources Research*, *42*(3), 1–5. https://doi.org/10.1029/2005wr004058

Brusseau, M. L., Peng, S., Schnaar, G., & Murao, A. (2007). Measuring air–water interfacial areas with X-ray microtomography and interfacial partitioning tracer tests. *Environmental Science & Technology*, *41*(6), 1956–1961. https://doi.org/10.1021/es061474m

Brusseau, M. L., Yan, N., Van Glubt, S., Wang, Y., Chen, W., Lyu, Y., et al. (2019). Comprehensive retention model for PFAS transport in subsurface systems. *Water Research*, *148*, 41–50. https://doi.org/10.1016/j.watres.2018.10.035

Chang, C.-H., & Franses, E. I. (1995). Adsorption dynamics of surfactants at the air/water interface: A critical review of mathematical models, data, and mechanisms. *Colloids and Surfaces A: Physicochemical and Engineering Aspects*, *100*, 1–45. https://doi.org/10.1016/0927-7757(94)03061-4

Costanza-Robinson, M. S., & Brusseau, M. L. (2002). Air-water interfacial areas in unsaturated soils: Evaluation of interfacial domains. *Water Resources Research*, *38*(10), 13-1. https://doi.org/10.1029/2001wr000738

Dauchy, X., Boiteux, V., Colin, A., Hémard, J., Bach, C., Rosin, C., & Munoz, J.-F. (2019). Deep seepage of per-and polyfluoroalkyl substances through the soil of a firefighter training site and subsequent groundwater contamination. *Chemosphere*, *214*, 729–737. https://doi.org/10.1016/j.chemosphere.2018.10.003

Davies, J. T. (1958). Adsorption of long-chain ions. I. *Proceedings of the Royal Society of London. Series A. Mathematical and Physical Sciences*, *245*(1242), 417–428.

Debye, P., & Hückel, E. (1923). De la theorie des electrolytes. I. abaissement du point de congelation et phenomenes associes. *Physikalische Zeitschrift*, *24*(9), 185–206.

Fainerman, V., & Lucassen-Reynders, E. (2002). Adsorption of single and mixed ionic surfactants at fluid interfaces. *Advances in Colloid and Interface Science*, *96*(1–3), 295–323. https://doi.org/10.1016/s0001-8686(01)00086-0

Glüge, J., Scheringer, M., Cousins, I. T., DeWitt, J. C., Goldenman, G., Herzke, D., et al. (2020). An overview of the uses of per-and poly-fluoroalkyl substances (PFAS). *Environmental Sciences: Processes & Impacts*, *22*(12), 2345–2373. https://doi.org/10.1039/d0em00291g

Gnesda, W. R., Draxler, E. F., Tinjum, J., & Zahasky, C. (2022). Adsorption of PFAAs in the vadose zone and implications for long-term groundwater contamination. *Environmental Science & Technology*, *56*(23), 16748–16758. https://doi.org/10.1021/acs.est.2c03962

Goss, K.-U. (2008). The pK_a values of PFOA and other highly fluorinated carboxylic acids. *Environmental Science & Technology*, *42*(2), 456–458. https://doi.org/10.1021/es8011904

Guo, B., Saleem, H., & Brusseau, M. L. (2023). Predicting interfacial tension and adsorption at fluid–fluid interfaces for mixtures of PFAS and/or hydrocarbon surfactants. *Environmental Science & Technology*, *57*(21), 8044–8052. https://doi.org/10.1021/acs.est.2c08601

Guo, B., Zeng, J., & Brusseau, M. L. (2020). A mathematical model for the release, transport, and retention of per-and polyfluoroalkyl substances (PFAS) in the vadose zone. *Water Resources Research*, *56*(2), e2019WR026667. https://doi.org/10.1029/2019wr026667

Guo, B., Zeng, J., Brusseau, M. L., & Zhang, Y. (2022). A screening model for quantifying PFAS leaching in the vadose zone and mass discharge to groundwater. *Advances in Water Resources*, *160*, 104102. https://doi.org/10.1016/j.advwatres.2021.104102

Guo, Y., & Yu, X. (2017). Characterizing the surface charge of clay minerals with atomic force microscope (AFM). *AIMS Materials Science*, *4*(3), 582–593. https://doi.org/10.3934/matersci.2017.3.582

Hamaker, H. C. (1937). The London–van der Waals attraction between spherical particles. *Physica*, *4*(10), 1058–1072. https://doi.org/10.1016/s0031-8914(37)80203-7

Israelachvili, J. N. (2011). *Intermolecular and surface forces*. Academic Press.

Iwatsu, M., & Horii, K. (1996). Capillary condensation and adhesion of two wetter surfaces. *Journal of Colloid and Interface Science*, *182*(2), 400–406. https://doi.org/10.1006/jcis.1996.0480

Jiang, H., Guo, B., & Brusseau, M. L. (2020). Pore-scale modeling of fluid-fluid interfacial area in variably saturated porous media containing microscale surface roughness. *Water Resources Research*, *56*(1), e2019WR025876. https://doi.org/10.1029/2019wr025876

Kalinin, V., & Radke, C. (1996). An ion-binding model for ionic surfactant adsorption at aqueous-fluid interfaces. *Colloids and Surfaces A: Physicochemical and Engineering Aspects*, *114*, 337–350. https://doi.org/10.1016/0927-7757(96)03592-3

Kissa, E. (2001). *Fluorinated surfactants and repellents* (Vol. 97). CRC Press.

Kralchevsky, P., Danov, K., Broze, G., & Mehreteab, A. (1999). Thermodynamics of ionic surfactant adsorption with account for the counterion binding: Effect of salts of various valency. *Langmuir*, *15*(7), 2351–2365. https://doi.org/10.1021/la981127t

Kretzschmar, R., Holthoff, H., & Sticher, H. (1998). Influence of pH and humic acid on coagulation kinetics of kaolinite: A dynamic light scattering study. *Journal of Colloid and Interface Science*, *202*(1), 95–103. https://doi.org/10.1006/jcis.1998.5440

Kroutil, O., Chval, Z., Skelton, A., & Predota, M. (2015). Computer simulations of quartz (101)–water interface over a range of pH values. *Journal of Physical Chemistry C*, *119*(17), 9274–9286. https://doi.org/10.1021/acs.jpcc.5b00096

Kumari, N., & Mohan, C. (2021). Basics of clay minerals and their characteristic properties. *Clays and Clay Minerals*, *24*, 1–29.

Le, S.-T., Gao, Y., Kibbey, T. C., Glamore, W. C., & O'Carroll, D. M. (2021). A new framework for modeling the effect of salt on interfacial adsorption of PFAS in environmental systems. *Science of the Total Environment*, *796*, 148893. https://doi.org/10.1016/j.scitotenv.2021.148893

Lemay, A. C., Sontarp, E. J., Martinez, D., Maruri, P., Mohammed, R., Neapole, R., et al. (2023). Molecular dynamics simulation prediction of the partitioning constants (K_H, K_{iw}, K_{ia}) of 82 legacy and emerging organic contaminants at the water–air interface. *Environmental Science & Technology*, *57*(15), 6296–6308. https://doi.org/10.1021/acs.est.3c00267

Li, Z., Lyu, X., Gao, B., Xu, H., Wu, J., & Sun, Y. (2021). Effects of ionic strength and cation type on the transport of perfluorooctanoic acid (PFOA) in unsaturated sand porous media. *Journal of Hazardous Materials*, *403*, 123688. https://doi.org/10.1016/j.jhazmat.2020.123688

Lyu, X., Liu, X., Sun, Y., Gao, B., Ji, R., Wu, J., & Xue, Y. (2020). Importance of surface roughness on perfluorooctanoic acid (PFOA) transport in unsaturated porous media. *Environmental Pollution*, *266*, 115343. https://doi.org/10.1016/j.envpol.2020.115343

Lyu, Y., & Brusseau, M. L. (2020). The influence of solution chemistry on air-water interfacial adsorption and transport of PFOA in unsaturated porous media. *Science of the Total Environment*, *713*, 136744. https://doi.org/10.1016/j.scitotenv.2020.136744

Lyu, Y., Brusseau, M. L., Chen, W., Yan, N., Fu, X., & Lin, X. (2018). Adsorption of PFOA at the air–water interface during transport in unsaturated porous media. *Environmental Science & Technology*, *52*(14), 7745–7753. https://doi.org/10.1021/acs.est.8b02348

Lyu, Y., Wang, B., Du, X., Guo, B., & Brusseau, M. L. (2022). Air-water interfacial adsorption of C4–C10 perfluorocarboxylic acids during transport in unsaturated porous media. *Science of the Total Environment*, *831*, 154905. https://doi.org/10.1016/j.scitotenv.2022.154905

Nakayama, S. F., Yoshikane, M., Onoda, Y., Nishihama, Y., Iwai-Shimada, M., Takagi, M., et al. (2019). Worldwide trends in tracing poly-and perfluoroalkyl substances (PFAS) in the environment. *TrAC, Trends in Analytical Chemistry*, *121*, 115410. https://doi.org/10.1016/j.trac.2019.02.011

Nishiyama, N., & Yokoyama, T. (2021). Water film thickness in unsaturated porous media: Effect of pore size, pore solution chemistry, and mineral type. *Water Resources Research*, *57*(6), e2020WR029257. https://doi.org/10.1029/2020wr029257

Olsson, D. M., & Nelson, L. S. (1975). The Nelder-Mead simplex procedure for function minimization. *Technometrics*, *17*(1), 45–51. https://doi.org/10.2307/1267998

Or, D., & Tuller, M. (1999). Liquid retention and interfacial area in variably saturated porous media: Upscaling from single-pore to sample-scale model. *Water Resources Research*, *35*(12), 3591–3605. https://doi.org/10.1029/1999wr900262

Potra, F. A., & Wright, S. J. (2000). Interior-point methods. *Journal of Computational and Applied Mathematics*, *124*(1–2), 281–302. https://doi.org/10.1016/s0377-0427(00)00433-7

Prausnitz, J. M., Lichtenthaler, R. N., & De Azevedo, E. G. (1998). *Molecular thermodynamics of fluid-phase equilibria*. Pearson Education.

Quinnan, J., Rossi, M., Curry, P., Lupo, M., Miller, M., Korb, H., et al. (2021). Application of PFAS-mobile lab to support adaptive characterization and flux-based conceptual site models at AFFF releases. *Remediation Journal*, *31*(3), 7–26. https://doi.org/10.1002/rem.21680

Rosen, M. J., & Kunjappu, J. T. (2012). *Surfactants and interfacial phenomena*. John Wiley & Sons.

Schaefer, C. E., Lavorgna, G. M., Lippincott, D. R., Nguyen, D., Christie, E., Shea, S., et al. (2022). A field study to assess the role of air-water interfacial sorption on PFAS leaching in an AFFF source area. *Journal of Contaminant Hydrology*, *248*, 104001. https://doi.org/10.1016/j.jconhyd.2022.104001

Silva, J. A. K., Šimůnek, J., & McCray, J. E. (2020). A modified hydrus model for simulating PFAS transport in the vadose zone. *Water*, *12*(10), 2758. https://doi.org/10.3390/w12102758

Singh, G., Kaur, G., Williard, K., Schoonover, J., & Kang, J. (2018). Monitoring of water and solute transport in the vadose zone: A review. *Vadose Zone Journal*, *17*(1), 1–23. https://doi.org/10.2136/vzj2016.07.0058

Sposito, G. (2016). *The chemistry of soils* (3rd ed.). Oxford university press.

Stern, O. (1924). Zur theorie der elektrolytischen doppelschicht. *Zeitschrift für Elektrochemie und Angewandte Physikalische Chemie*, *30*(21–22), 508–516. https://doi.org/10.1002/bbpc.192400182

Tajima, K. (1970). Radiotracer studies on adsorption of surface active substance at aqueous surface. II. The effect of excess salt on the adsorption of sodium dodecylsulfate. *Bulletin of the Chemical Society of Japan*, *43*(10), 3063–3066. https://doi.org/10.1246/bcsj.43.3063

Tajima, K., Muramatsu, M., & Sasaki, T. (1970). Radiotracer studies on adsorption of surface active substance at aqueous surface. I. accurate measurement of adsorption of tritiated sodium dodecylsulfate. *Bulletin of the Chemical Society of Japan*, *43*(7), 1991–1998. https://doi.org/10.1246/bcsj.43.1991

Tokunaga, T. K. (2011). Physicochemical controls on adsorbed water film thickness in unsaturated geological media. *Water Resources Research*, *47*(8), W08514. https://doi.org/10.1029/2011wr010676

Tokunaga, T. K. (2012). DLVO-based estimates of adsorbed water film thicknesses in geologic CO_2 reservoirs. *Langmuir*, *28*(21), 8001–8009. https://doi.org/10.1021/la2044587

Tuller, M., Or, D., & Dudley, L. M. (1999). Adsorption and capillary condensation in porous media: Liquid retention and interfacial configurations in angular pores. *Water Resources Research*, *35*(7), 1949–1964. https://doi.org/10.1029/1999wr900098

Vassilieff, S. C., Tenchov, B., Grigorov, L., & Richmond, P. (1983). Electrostatic disjoining pressure in symmetrical films with adsorptive charge regulation. *Journal of Colloid and Interface Science*, *93*(1), 8–17. https://doi.org/10.1016/0021-9797(83)90378-8

Verwey, E. J. W., & Overbeek, J. T. G. (1955). Theory of the stability of lyophobic colloids. *Journal of Colloid Science*, *10*(2), 224–225. https://doi.org/10.1016/0095-8522(55)90030-1

Wallis, I., Hutson, J., Davis, G., Kookana, R., Rayner, J., & Prommer, H. (2022). Model-based identification of vadose zone controls on PFAS mobility under semi-arid climate conditions. *Water Research*, *225*, 119096. https://doi.org/10.1016/j.watres.2022.119096

Zeng, J., & Guo, B. (2021). Multidimensional simulation of PFAS transport and leaching in the vadose zone: Impact of surfactant-induced flow and subsurface heterogeneities. *Advances in Water Resources*, *155*, 104015. https://doi.org/10.1016/j.advwatres.2021.104015

Zeng, J., Brusseau, M. L., & Guo, B. (2021). Model validation and analyses of parameter sensitivity and uncertainty for modeling long-term retention and leaching of PFAS in the vadose zone. *Journal of Hydrology*, *603*, 127172. https://doi.org/10.1016/j.jhydrol.2021.127172

Zhang, W., & Guo, B. (2023). Anomalous adsorption of PFAS at the thin-water-film air–water interface in water-unsaturated porous media (version 5) [Dataset]. Zenodo. https://doi.org/10.5281/zenodo.10086205

References From the Supporting Information

Brusseau, M. L. (2023). Determining air-water interfacial areas for the retention and transport of PFAS and other interfacially active solutes in unsaturated porous media. *Science of the Total Environment*, *884*, 163730. https://doi.org/10.1016/j.scitotenv.2023.163730

Fainerman, V., Lucassen-Reynders, E., & Miller, R. (2003). Description of the adsorption behaviour of proteins at water/fluid interfaces in the framework of a two-dimensional solution model. *Advances in Colloid and Interface Science*, *106*(1–3), 237–259. https://doi.org/10.1016/s0001-8686(03)00112-x

Gregory, J. (1975). Interaction of unequal double layers at constant charge. *Journal of Colloid and Interface Science*, *51*(1), 44–51. https://doi.org/10.1016/0021-9797(75)90081-8

Kirkwood, J. (1961). *Oppenheim, chemical thermodynamics*. McGraw-Hill.

Lucassen-Reynders, E. (1966). Surface equation of state for ionized surfactants. *The Journal of Physical Chemistry*, *70*(6), 1777–1785. https://doi.org/10.1021/j100878a016

van Genuchten, M. T. (1980). A closed-form equation for predicting the hydraulic conductivity of unsaturated soils. *Soil Science Society of America Journal*, *44*(5), 892–898. https://doi.org/10.2136/sssaj1980.03615995004400050002x